Optical Engineering

SPIEDigitalLibrary.org/oe

Thermal damages on the surface of a silicon wafer induced by a near-infrared laser

Sungho Choi
Kyung-Young Jhang

SPIE

Thermal damages on the surface of a silicon wafer induced by a near-infrared laser

Sungho Choi and Kyung-Young Jhang*
Hanyang University, Graduate School of Mechanical Engineering, Seoul 133-791, Republic of Korea

Abstract. Laser-induced thermal damages of a silicon wafer surface subjected to continuous near-infrared laser irradiation were investigated. Silicon wafer specimens were illuminated by a continuous-wave fiber laser beam (1070-nm wavelength) with irradiances from 93 to 186 W/cm^2, and the surface morphology of each specimen was analyzed using optical microscopy. With increasing irradiance, straight cracks in the <110> direction appeared first, and partial melting and complete melting were subsequently observed. The mechanism of these laser-induced thermal damages in the silicon wafer surface was discussed with numerical analysis based on the heat transfer and thermoelasticity model. The irradiances initiating the cracking and melting were predicted by determining the irradiances in which the calculated thermal stress and temperature exceeded the corresponding limits of the fracture strength and melting point, respectively. These predictions agreed well with the experimental findings. Laser-induced thermal damages of the silicon wafer surface subjected to a continuous near-infrared laser irradiation were identified based on these investigations. [DOI: 10.1117/1.OE.53.1.017103]

Keywords: near-infrared laser; laser-induced thermal damages; silicon; cracking; melting.

Paper 131382 received Sep. 6, 2013; revised manuscript received Nov. 13, 2013; accepted for publication Dec. 16, 2013; published online Jan. 10, 2014.

1 Introduction

The use of continuous wave (CW) lasers with a wavelength of ~1070 nm nm has recently increased for a directed energy weapon because these lasers have less attenuation in the atmosphere than ultraviolet or visible wavelength lasers.[1,2] Generally, the target is damaged by the thermal effect of the laser energy absorbed into the target material.

Previous investigations of laser-induced thermal damages by laser weapons have focused primarily on missile, rocket, aircraft, and unmanned aerial vehicles.[3–8] In this case, the high power of a laser beam or long exposure time is necessary to induce thermal damage on the target surface in order to increase the temperature to the melting or vaporization point. In general, a hard-kill laser weapon requires 100 kW. However, if an electro-optic/infrared system is exposed to laser beam irradiation, the system can easily break down due to cracking or melting damage of the optics and sensor components at a lower power than in the case of a metallic structure.[9–11] That is, optical systems are specifically weaker to laser attack.

Silicon is normally used as a substrate material in optical elements and photodetectors. Optically, silicon has a low absorption coefficient less than 10^{-7} cm^{-1} at 1.2 to 7 and 25 to 300 μm light wavelengths; therefore, a very small portion of the laser energy is absorbed, and most laser energy is transmitted at these wavelength ranges. However, much more laser energy can be absorbed at other wavelengths. For example, at a 1070-nm wavelength, the absorption coefficient is 10 cm^{-1} and the absorbance is 0.278 at a thickness of 525 μm.[12] Moreover, the absorption coefficient rapidly increases with an increase in temperature. Therefore, silicon is very vulnerable to a near-infrared (NIR) laser with a wavelength of approximately 1070 nm.

Even though prestigious achievements in laser-induced thermal damages in silicon crystals have been reported in the field of laser processing technology, most studies focused on the ablation effect induced by ultraviolet (UV) and visible (VIS) wavelength lasers,[13–16] and a few researchers have explained cracking and melting damage induced by an NIR laser.[17,18]

In this paper, the thermal damages in silicon wafers, such as cracking and melting, induced by an NIR CW laser beam with a 1070-nm wavelength were investigated under various irradiances. Czochralski-grown, single crystal silicon p-type (100) plane specimens were illuminated by a 1070-nm fiber laser, and the surface morphology of specimens after irradiation was observed using an optical microscope (OM) to analyze the cracking and melting damage. In order to identify the damage mechanism, numerical simulations were performed to predict the irradiances that initiate the cracking and melting, and the predicted irradiances were compared with experimental findings. In the simulation, the thermal stress and temperature variations induced by the NIR CW laser were calculated based on the heat transfer and thermoelasticity model.[19–21] The cracking damage was predicted by comparing the calculated thermal stress with the fracture strength of silicon, and the melting damage was predicted by comparing the calculated temperature with the melting point of silicon.

2 Experimental Procedures

A schematic diagram of the experimental system is shown in Fig. 1. Czochralski-grown, single crystal silicon p-type (100) plane specimens with a thickness of 525 $\pm$ 25 μm were illuminated by a CW fiber laser (IPG photonics, 1070-nm wavelength, 1-kW maximum laser beam power, and 5.85-mm

*Address all correspondence to: Kyung-Young Jhang, E-mail: kyjhang@hanyang.ac.kr

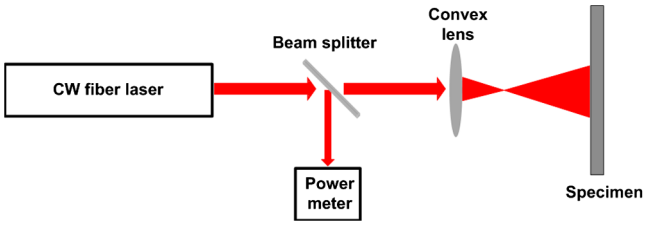

Fig. 1 Schematic diagram of the experimental system.

laser beam diameter). A quartz beam splitter, reflecting 10% of the laser beam energy to a power meter, was used to monitor the laser beam power. A laser beam with an 11.7-mm diameter irradiated the specimens for 20 s. Although the practical attack time will be a few seconds in the military application, in order to consider the effect of thermal convection and radiation that suppress the temperature rise, we have tested enough long time exposure until the temperature and stress are mostly saturated. The laser power increased from 100 to 200 W in 10 W steps, which correspond to irradiances ranging from 93 to 186 W/cm^2 in 9 W/cm^2 steps. The tests were performed six times at each laser power. The surface morphology of the silicon specimens subjected to the laser beam was analyzed using an optical microscope.

3 Experimental Results

Figure 2 shows the OM images of the silicon wafer surface before and after laser irradiation at a 121 W/cm^2 irradiance, where Fig. 2(a) is the clean surface before laser irradiation and Fig. 2(b) is the cracked surface after. Surface cracks appeared in the $x[110]$ and y directions $[\bar{1}10]$ [Fig. 2(b)] because these directions are the weakest in the single-crystal silicon (100) plane.[22] Surface cracks were observed at 121 W/cm^2 irradiance or greater, while no cracks were observed at an irradiance of 112 W/cm^2 or less.

Figure 3(a) shows the schematic diagram of the silicon wafer surface when the irradiance of the laser beam was 139 W/cm^2. A partially melted zone appeared. Figure 3(b) shows the OM image of the silicon wafer surface near the center of the laser beam spot. The surface morphology is significantly varied due to partial surface melting. This surface morphology was formed by cracks generated prior to melting. Multiple reflections and absorptions of the laser beam at the crack increased the absorption, causing melting to occur first along the crack.[23] Figure 3(c) shows the OM image of the "A" zone in Fig. 3(a), which is the boundary of the melted area. A partially melted zone and surface cracks were observed. The boundary of the partially melted zone showed an orthogonal shape because melting easily occurred in the crack. The irradiances-inducing partial melting was 130 and 139 W/cm^2.

Figure 4(a) shows the schematic diagram of the silicon wafer surface when the irradiance of the laser beam was 149 W/cm^2. A completely melted zone was observed at the center of the laser beam spot, and a partially melted zone and cracks were observed at the outside. Figure 4(b) shows the OM image of the "B" zone in Fig. 4(a), which is the boundary of complete and partial melting. As the irradiance of the laser beam increased, the center of the partially melted zone shown in Fig. 3(b) dissolved entirely and became flat. A completely melted zone was observed at an irradiance of 149 W/cm^2 or greater. A summary of these experimental results is shown in Table 1.

4 Discussion of the Damage Mechanism using Numerical Analysis

In order to identify the damage mechanism, numerical analysis was performed based on the heat transfer and thermoelasticity model. First, the thermal stress was calculated at various laser irradiances, and the cracking irradiance was predicted by determining the irradiance at which the calculated von mises stress exceeded the fracture strength. The temperature was then calculated at various laser irradiances, and the melting irradiance was predicted by determining the irradiance at which the calculated temperature exceeded the melting point. These predictions were compared with the experimental results.

The thermal stress variation in specimens subjected to laser irradiation was obtained from the solution of the Duhamel-Neumann law for linear elasticity, which considers the effect of thermal expansion as follows:[19]

$$\sigma_{ij} = C_{ijkl}\varepsilon_{kl} - \beta_{ij}(T - T_0), \tag{1}$$

where σ is the stress, C is the elastic constant, ε is the strain, β is the thermal modulus, T is the temperature, and T_0 is the initial temperature.

In Eq. (1), the transient temperature distribution $T(x, y, z, t)$ can be obtained using a classical heat conduction

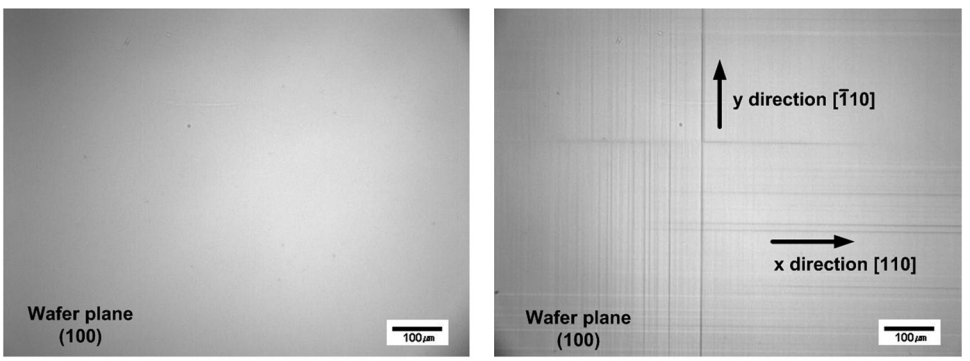

(a) (b)

Fig. 2 OM images of the silicon wafer surface (a) before and (b) after laser beam irradiation at 121 W/cm^2. The cracks were generated in the $x[110]$ and $y[\bar{1}10]$ directions.

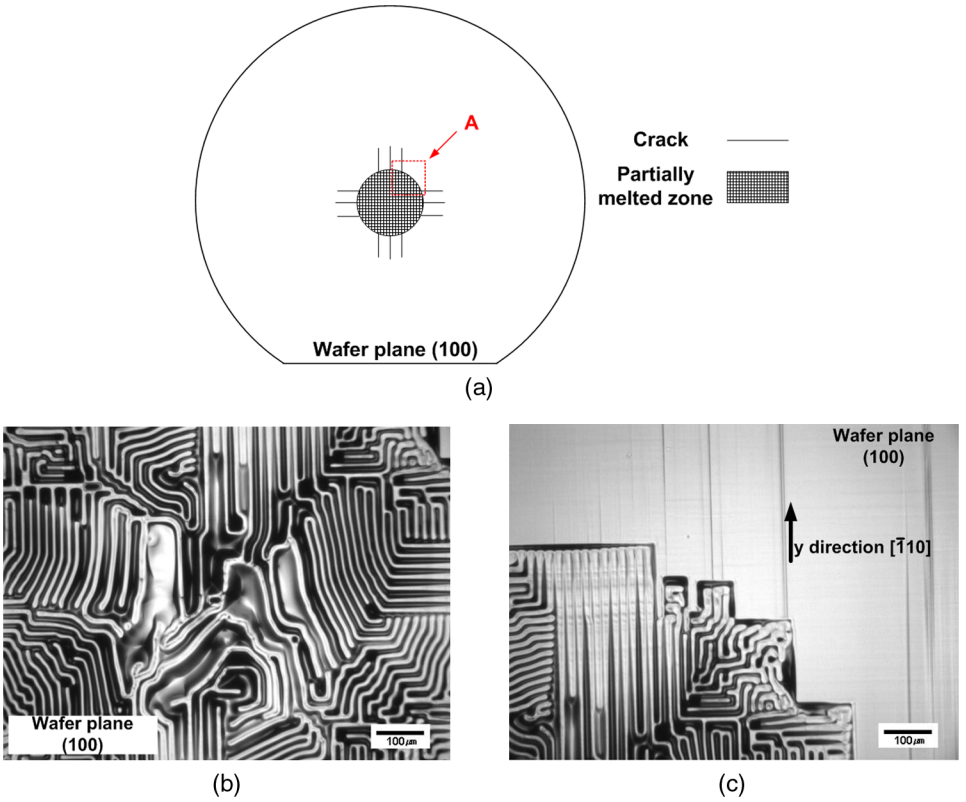

Fig. 3 (a) Schematic diagram of the silicon wafer surface at an irradiance of 139 W/cm^2, (b) OM image of the silicon wafer surface near the center of the laser beam spot and (c) OM image of the "A" zone in (a).

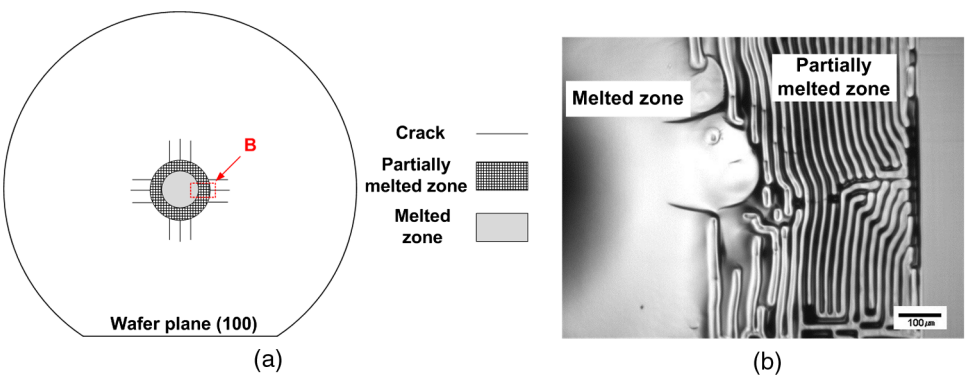

Fig. 4 (a) Schematic diagram of the silicon wafer surface at the irradiance of 149 W/cm^2 and (b) OM image of the "B" zone in (a).

Table 1 Summary of the experimental results.

Irradiance (W/cm^2)	≤112	121	130	139	≥ 149
Typical OM image			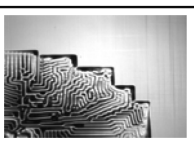	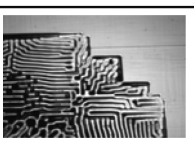	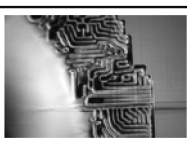
Damage	No damage	Cracking	Partial melting	Partial melting	Complete melting

analysis. The three-dimensional (3-D) differential equation of the heat conduction is given as follows:[20]

$$\rho C_p \frac{\partial T}{\partial t} - \nabla(k\nabla T) = Q, \tag{2}$$

where ρ is the density, C_p is the heat capacity, k is the thermal conductivity, and Q is the heat source per unit volume as a function of position and time.

The heat source per unit volume Q can be represented as the incident laser intensity. Assuming that the spatial distribution of the laser beam is Gaussian, the heat source per unit volume Q can be expressed as follows:[21]

$$Q = I_0(1-R)\gamma \exp(-\gamma z) \exp\left(-2\frac{x^2+y^2}{r_0^2}\right), \tag{3}$$

where I_0 is the intensity of the incident beam, R is the reflectivity, γ is the absorption coefficient, and r_0 is the radius of the laser beam, which is defined as the radial distance at which the intensity decreases to e^{-2} of I_0.

The thermal stress and temperature variations of a silicon wafer induced by CW laser irradiation were simulated with a 3-D one fourth symmetric model using COMSOL Multiphysics. Figure 5 shows the simulation model of the silicon specimen irradiated by a CW laser beam. The radius of the specimen was 50.8 mm, and the symbol "D" denotes the volume of the heat source. A boundary condition of "E" is symmetric. The other boundary is traction-free, where convection and radiation into the ambient were given as follows:

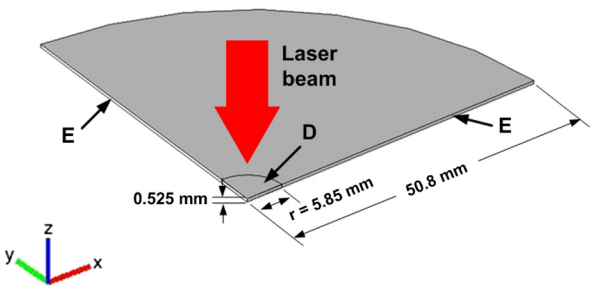

Fig. 5 Simulation model of the silicon wafer subjected to a CW laser beam. The symbol "D" denotes the heat source volume, and the symbol "E" indicates the symmetric boundary. The specimen dimensions are given.

$$\mathbf{n} \cdot (k\nabla T) = h(T_{\text{amb}} - T) + \varepsilon_{\text{rad}}\sigma_{\text{SB}}(T_{\text{amb}}^4 - T^4), \tag{4}$$

where n is the normal vector of the boundary, h is the convective heat transfer coefficient, T_{amb} is the ambient temperature, ε_{rad} is the emissivity, and σ_{SB} is the Stefan–Boltzmann constant.

The NIR CW laser with a 1070-nm wavelength used in this model has a Gaussian beam shape. The radius of the laser beam was 5.85 mm. The temperature-dependent physical and optical properties of the silicon, including density, thermal conductivity, heat capacity, thermal expansion coefficient, Young's modulus, Poisson's ratio, absorption coefficient and reflectivity, are given in Table 2.[12,17,24] A time-dependent solver was used, and the solid–liquid phase change in the silicon was considered in terms of the specific heat capacity.[20] The calculation duration time was 20 s in 0.01 s intervals, and the initial temperature of the silicon wafer was 20°C.

Simulation results for the profiles of typical stresses σ_{xx}, σ_{yy}, σ_{zz}, and σ_v (von mises stress) on the surface of silicon specimen subjected to a laser irradiance of 121 W/cm^2 for 20 s are shown in Fig. 6. The tensile stress is positive and the compressive stress is negative. For the stresses σ_{xx} and σ_{yy}, the maximum compressive stress is located at the center of the laser beam spot with the approximate value of 215 MPa. On the other hand, the maximum stress of σ_{zz} is only 1.5 MPa which is very small compared with the other stresses. This means that the effect of stress σ_{zz} is negligible. For the von mises stress σ_v, the maximum stress is located at the center of the laser beam spot with the approximate value of 214 MPa.

The variation of the von mises stress (σ_v) at the center of the laser beam for irradiances of 112, 121, 130, and 139 W/cm^2 is shown in Fig. 7. To predict the cracking occurrence, the stress variation was compared with the fracture strength. In general, the fracture strength of silicon depends on the specimen size and thickness. Moreover, the fracture strength has large deviations due to the brittle fracture behavior. Paul et al.[25] statistically studied the fracture strength of silicon with varying thicknesses using Weibull and normal models. The fracture strength of silicon

Table 2 Physical and optical properties of a silicon wafer depending on temperature.

Temperature (°C)	20	220	420	620	820	1020	1220
Density (kg/m^3)	2330.0	2325.6	2320.3	2314.5	2308.3	2301.2	2292.0
Thermal conductivity [W/(m°C)]	159.3	81.5	49.6	34.8	27.5	24.6	23.4
Heat capacity (J/(kg°C))	708.8	795.8	865.1	903.6	956.6	996.7	1018.8
Thermal expansion coefficient (10^{-6}/°C)	2.57	3.60	4.06	4.22	4.33	4.45	4.57
Young's modulus (GPa)	130.7	124.9	119.0	113.1	107.6	95.4	89.8
Poisson's ratio	0.2763	0.2762	0.2761	0.2760	0.2759	0.2758	0.2757
Absorption coefficient (1/cm)	10	87	370	1088	2570	5249	9673
Reflectivity	0.319	0.322	0.330	0.338	0.347	0.357	0.367

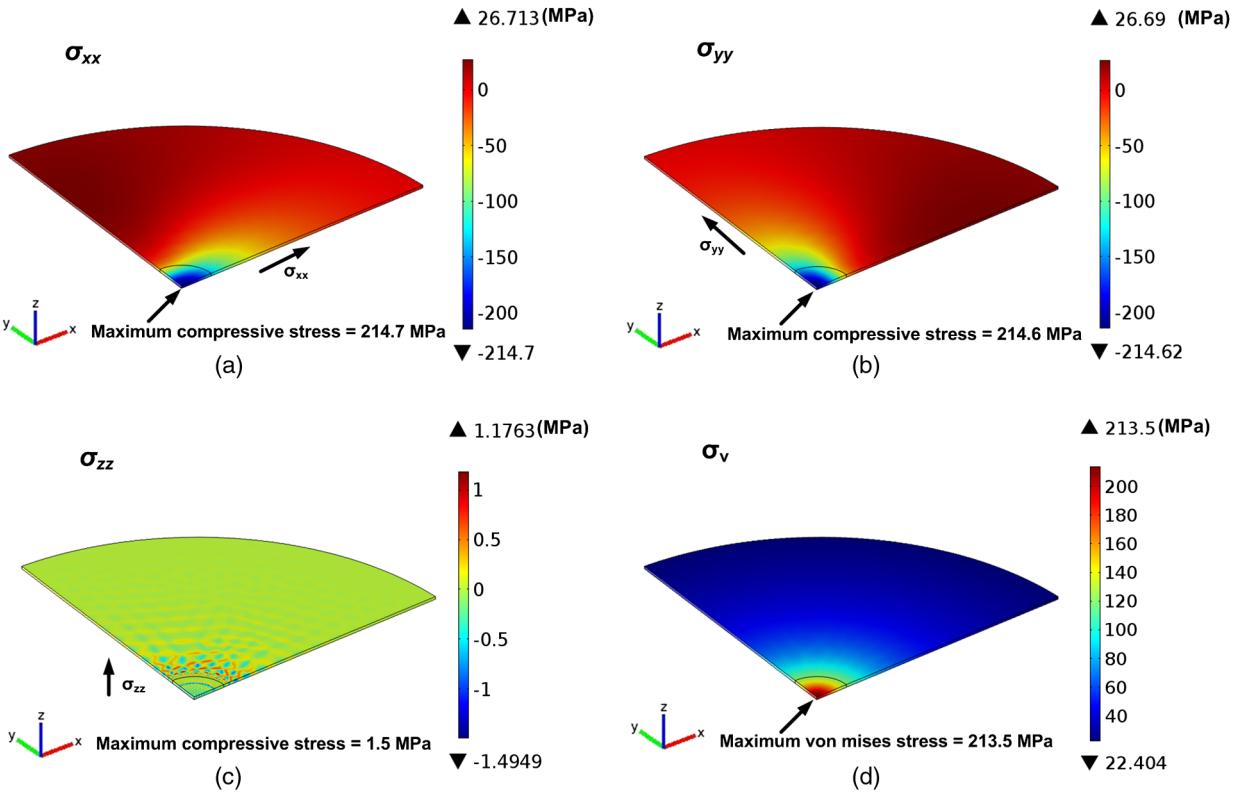

Fig. 6 Simulation results for the profiles of stresses [(a) σ_{xx}, (b) σ_{yy}, (c) σ_{zz}, and (d) σ_v] on the surface of silicon specimen subjected to a laser irradiance of 121 W/cm^2 for 20 s.

with a thickness of 525 μm ranged from 96 to 386 MPa with a nearly normal distribution (average fracture strength of 222 MPa and a standard deviation of 70 MPa). As a result, the fracture strength range of 222 $\pm$ 20 MPa was adopted, which has a high probability density. This range is shown as a band in Fig. 7. Assuming that the cracking occurred when the von mises stress reached the range of the fracture strength, the cracking is predicted to be initiated when the laser irradiance is greater than 121 W/cm^2 for 20 s. These results agree well with experimental findings.

In this study, we have tested enough long time exposure until the stress and temperature were mostly saturated by the effect of thermal convection and radiation. In practice, in military applications, however, a shorter time exposure with higher laser irradiance may be interesting. Even in such a case, our simulation scheme is still available, since the damage mechanism is not changed when the irradiation time is only longer than a millisecond.

The temperature variation at the center of the laser beam for irradiances of 112, 121, 130, and 139 W/cm^2 is shown in Fig. 8. The temperature increased sharply at the beginning of the laser beam irradiation and then slowly increased due to the effects of convection and radiation. The maximum temperature was ~935, 1015, 1090, and 1155°C after 20 s, respectively, and all of these temperatures were below the melting point of silicon (1412°C). Therefore, melting is not expected to occur in these cases.

To predict the melting occurrence, a simulation was performed with the stronger laser beam irradiance of

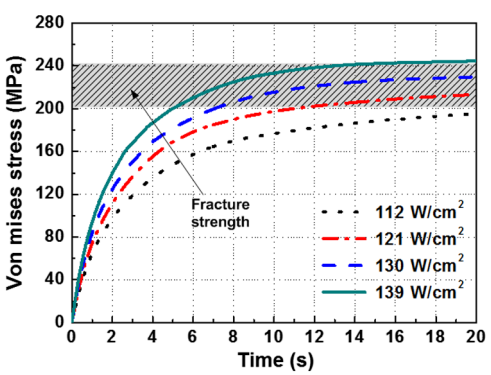

Fig. 7 Simulation results for the von mises stress σ_v variation at the center of the laser beam for irradiances of 112, 121, 130, and 139 W/cm^2.

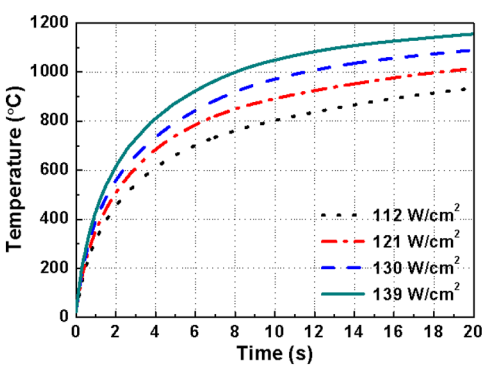

Fig. 8 Simulation results for the temperature variation at the center of the laser beam for irradiances of 112, 121, 130, and 139 W/cm^2.

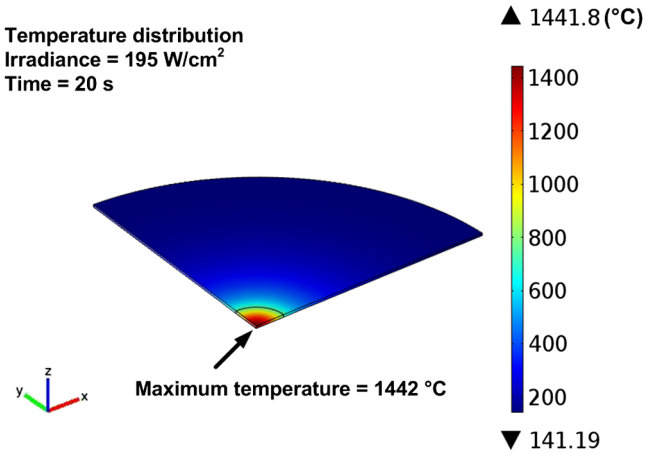

Fig. 9 Simulation result for the temperature distribution on a silicon specimen subjected to a laser irradiance of 195 W/cm^2 for 20 s.

195 W/cm^2. The simulation result for the temperature distribution on the silicon specimen subjected to a laser beam irradiation for 20 s is shown in Fig. 9. The temperature at the center of the laser beam increased to 1442°C, which was greater than the melting point of silicon. Therefore, melting is expected to occur when a laser beam with irradiance of 195 W/cm^2 or greater irradiates the silicon wafer for 20 s.

However, partial melting was observed at the lower irradiances, which is reasonable when considering the increase in absorbance of laser energy by multiple reflections and absorptions in the cracks.[23] In the simulation model, the absorption of the laser beam was supposed to occur only once. But if surface cracks appeared during the laser beam irradiation, the absorbance of the laser energy is increased by multiple reflections and absorptions. Therefore, in the experiments, surface melting occurred at the lower irradiances than the numerically predicted irradiance.

5 Conclusions

Laser-induced thermal damages, such as cracking and melting, on the silicon wafer surface subjected to the irradiation of a 1070-nm wavelength NIR CW laser were investigated by experiments and numerical simulations. Czochralski-grown, single crystal silicon p-type (100) plane specimens were illuminated by a CW fiber laser at various irradiances for 20 s, and the surface morphology of specimens after irradiation was analyzed using an OM. With the increase in irradiance, surface cracks appeared first and then subsequent partial and complete melting occurred. Surface cracks occurred in the <110> direction because this direction is the weakest in the (100) plane. Melting occurred first along the crack because the absorption of laser energy increased at the crack due to multiple reflections and absorptions. This formed a partially melted zone. As the irradiance is further increased, the surface was entirely melted. The irradiances responsible for initiating a crack, partial melting and complete melting were 121, 130 and 149 W/cm^2, respectively.

These values were compared with the numerical predictions to verify that experimentally observed damages, such as cracking and melting, were induced by thermal stress and increased temperature. A numerical calculation model was based on the heat transfer and thermoelasticity. The cracking irradiance was predicted by determining the irradiance that the calculated von mises stress reached the fracture strength range, 222 ± 20 MPa, and the melting irradiance was predicted by finding the temperature at which the calculated temperature exceeds the melting point, 1442°C. The predicted cracking irradiance was identical to the experimental result. However, numerical prediction for initiating surface melting was 195 W/cm^2, which is greater than the experimental observation. Nevertheless, this is reasonable when considering the absorbance of the laser energy increased due to the multiple reflection and absorptions at the cracks induced prior to the melting so that the melting occurred at a lower irradiance than the numerically predicted value.

Based on these investigations, laser-induced thermal damages of a silicon wafer surface subjected to CW NIR laser irradiation were identified.

Acknowledgments

This work was supported by the research fund of the Survivability Technology Defense Research Center of Agency for Defense Development of Korea (No. UD120019OD).

References

1. Y. Kalisky and O. Kalisky, "Applications and performance of high power lasers and in the battlefield," *Opt. Mater.* **34**(2), 457–460 (2011).
2. J. Zhang et al., "Crystal growth, optical properties, and CW laser operation at 1.06 μm of Nd:GAGG crystals," *Laser Phys. Lett.* **6**(5), 355–358 (2009).
3. P. V. Zarubin, "Academician Basov, high–power lasers, and the anti-missile defense problem," *Opt. Eng.* **52**(2), 021002 (2013).
4. J. Cook, "High–energy laser weapons since the early 1960s," *Opt. Eng.* **52**(2), 021007 (2013).
5. D. H. Kiel, "Is this the time for a high–energy laser weapon program?," *Opt. Eng.* **52**(2), 021008 (2013).
6. S. Ghoshroy, "Coming not so soon to a theater near you: laser weapons for missile defense," *B. Atom. Sci.* **67**(6), 34–43 (2011).
7. Y. Kalisky and O. Kalisky, "The status of high-power lasers and their applications in the battlefield," *Opt. Eng.* **49**(9), 091003 (2010).
8. M. Lavan, "High energy laser systems for short range defense," *Acta Phys. Pol. A* **115**(6), 959–963 (2009).
9. K. H. Lee, W. S. Shin, and E. C. Kang, "Analysis of optical damage in germanium induced by a continuous wave laser," *Appl. Opt.* **52**(10), 2055–2061 (2013).
10. Y. Liu, "Research on laser weapon soft damage to IR seeker," *J. Comput.* **6**(6), 1238–1245 (2011).
11. J. Xu et al., "Laser-jamming analysis of combined fiber lasers to imaging CCD," *Opt. Laser. Eng.* **47**(7–8), 800–806 (2009).
12. C. J. Fu and Z. M. Zhang, "Nanoscale radiation heat transfer for silicon at different doping levels," *Int. J. Heat Mass Transf.* **49**(9–10), 1703–1718 (2006).
13. J. Thorstensen and S. E. Foss, "Temperature dependent ablation threshold in silicon using ultrashort laser pulses," *J. Appl. Phys.* **112**(10), 103514 (2012).
14. S. Tao et al., "Thermal modeling and experimental study of infrared nanosecond laser ablation of silicon," *J. Appl. Phys.* **106**(12), 123507 (2009).
15. D. M. Karnakis, "High power single-shot laser ablation of silicon with nanosecond 355 nm," *Appl. Surf. Sci.* **252**(22), 7823–7825 (2006).
16. J. H. Yoo et al., "Explosive change in crater properties during high power nanosecond laser ablation of silicon," *J. Appl. Phys.* **88**(3), 1638–1649 (2000).
17. X. Wang et al., "Numerical and experimental study of the thermal stress of silicon induced by a millisecond laser," *Appl. Opt.* **50**(21), 3725–3732 (2011).
18. J. Liu et al., "Thermal stress cleaving of silicon wafer by pulsed Nd: YAG laser," *Chin. Opt. Lett.* **8**(10), 1000–1003 (2010).
19. I. A. Veres, T. Berer, and P. Burgholzer, "Numerical modeling of thermoelastic generation of ultrasound by laser irradiation in the coupled thermoelasticity," *Ultrasonics* **53**(1), 141–149 (2013).
20. Z. Said–Bacar et al., "Modeling of CW laser diode irradiation of amorphous silicon films," *Appl. Surf. Sci.* **257**(12), 5127–5131 (2011).
21. M. Alimardani, E. Toyserkani, and J. P. Huissoon, "A 3D dynamic numerical approach for temperature and thermal stress distributions

in multilayer laser solid freeform fabrication process," *Opt. Laser. Eng.* **45**(12), 1115–1130 (2007).
22. R. F. Cook, "Strength and sharp contact fracture of silicon," *J. Mater. Sci.* **41**(3), 841–872 (2006).
23. S. H. Choi et al., "Surface characteristics of aluminum 6061-T6 subjected to Nd:YAG pulsed-laser irradiation," *J. Mech. Sci. Technol.* **26**(7), 2163–2166 (2012).
24. N. M. Ravindra et al., "Emissivity measurements and modeling of silicon–related materials: an overview," *Int. J. Thermophys.* **22**(5), 1593–1611 (2001).
25. I. Paul et al., "Statistical fracture modelling of silicon with varying thickness," *Acta Mater.* **54**(15), 3991–4000 (2006).

Sungho Choi received his BS in mechanical engineering from Hanyang University, Seoul, Korea in 2010. He is currently working on his MS/PhD at Hanyang University, Seoul, Korea studying laser-material interactions and ultrasonic nondestructive evaluation methods.

Kyung-Young Jhang received BS and MS degrees in precision mechanical engineering from Hanyang University, Seoul, Korea, in 1983 and 1985, respectively. In 1991, he received a PhD in precision mechanical systems from the Tokyo Institute of Technology, Yokohama, Japan. He has been a professor at Hanyang University, Seoul, Korea since 1992. His research interests are experimental mechanics, ultrasonic nondestructive evaluation, optical measuring system, visual image processing, random signal processing, and laser-material interaction.